DISCLAIMER

This report was prepared as an account of work sponsored by an agency of the United States Government. Neither the United States Government nor any agency thereof, nor any of their employees, makes any warranty, express or implied, or assumes any legal liability or responsibility for the accuracy, completeness, or usefulness of any information, apparatus, product, or process disclosed, or represents that its use would not infringe privately owned rights. Reference herein to any specific commercial product, process, or service by trade name, trademark, manufacturer, or otherwise does not necessarily constitute or imply its endorsement, recommendation, or favoring by the United States Government or any agency thereof. The views and opinions of authors expressed herein do not necessarily state or reflect those of the United States Government or any agency thereof. Reference herein to any social initiative (including but not limited to Diversity, Equity, and Inclusion (DEI); Community Benefits Plans (CBP); Justice 40; etc.) is made by the Author independent of any current requirement by the United States Government and does not constitute or imply endorsement, recommendation, or support by the United States Government or any agency thereof.

Determining the transient electric field and the effect of pulse repetition frequency on the field in a repetitive 10-ns pulsed discharge in a quiescent CH_4-air mixture

Introduction

The goal of this research is to understand the underlying physics enabled by nanosecond pulsed power in a discharge initiation and the following physicochemical processes that favor lean-fuel plasma ignition for combustion. The hypothesis of this project is that pulsed power waveforms such as the pulse repetition frequency, voltage amplitude, and dielectric surface alter the reduced electric field during the initiation of the discharge, resulting in different plasma properties, which will vary the physicochemical processes for efficient and selective radical productions. This is especially important for lean-burn combustion and reducing emission.

Accomplishments

1. This low-temperature plasma research (PRF) facility project was to enable research on electric field measurements for nanosecond pulsed plasma sources for transient plasma ignition (TPI) for combustion with collaborations between researchers of ODU and Sandia. In addition to advancing low-temperature plasma science with quantitative information about the effects of the pulsed power parameters on the electric field distribution and kinetics in TPI, this project provides valuable opportunity to train next generation researchers in the field. A 3rd year PhD student from ODU and the PI have both traveled to Sandia National Labs at Livermore for on-site experiments. The student has gained lots of experience on the advanced laser diagnostic technique at Sandia and is currently scheduled to defend for PhD degree this December.
2. This travel-supporting project facilitated our previous collaboration with researchers at Sandia National Laboratories (Livermore, CA) on investigating the plasma properties and behaviors during the transient plasma ignition (TPI) for combustion. The effect of transient plasma modes on ignition kernel development was investigated for a quiescent CH_4-air combustion model system. A sustained ignition kernel expansion was observed when the plasma discharge transitioned into a transient spark or spark discharge. Employing repetitive 10-pulse sequence at 10 kHz was found being able to extend the lean-fuel limit of a single-pulse or lower frequency ignition. Details of the finding was reported in a peer-reviewed journal publication:

Peer-reviewed publication:

- C. Jiang, et al., "On the modes of nanosecond pulsed plasmas for combustion ignition of quiescent CH_4-air mixtures, J. Phys. D: Appl. Phys. 2024. 57, 435203, https://doi.org/10.1088/1361-6463/ad6876.

3. The spatiotemporal quantification of the electric field (**E**) in a pin-to-pin configuration powered by 10-ns pulsed high voltage pulses in a quiescent CH_4/air mixtures at 1 bar was determined using the electric field-induced second harmonic generation (EFISH) technique. Effects of pulse repetition frequency, the equivalence ratio, and dielectric surface between the pin electrodes on **E** were evaluated. Up to 66 kV/cm of **E** (or 270 Td of the reduced electric field assuming the gas temperature at room temperature) was measured as the field needed to achieve a spark discharge and sustain ignition kernel. Increasing the pulse repetition frequency lowers E for transient spark but increases the reduced electric field due to the elevated gas temperature. Findings from the

research were presented in international conferences as well as submitted for a peer-reviewed journal publication.

Conference presentations:

- M. Z. Rahman, et al., "Determining the electric field in a 10-ns pulsed plasma in methane-air mixture using E-FISH," *The 2024 IEEE International Power Modulator and High Voltage Conference*, Indianapolis, IN, May 30, 2024.
- M. Z. Rahman, et al., "Impact of the dielectric surface on the electric field in a 10-ns transient plasma in a CH_4-air mixture," The 77th Annual Gaseous Electronics Conference, San Diego, CA, Oct 1st, 2024.
- M. Z. Rahman, et al., "Determining the electric field in a 10-ns pulsed discharge in a CH_4-air mixture using EFISH," The 77th Annual Gaseous Electronics Conference, San Diego, CA, Oct 3rd, 2024.

Peer-reviewed publications:

- M. Z. Rahman, et al., "Determining the electric field in a 10-ns pulsed plasma in fuel-air mixtures using EFISH," submitted to Plasma Sources Science and Technology, in review.

OPEN ACCESS
IOP Publishing
Journal of Physics D: Applied Physics
J. Phys. D: Appl. Phys. **57** (2024) 435203 (13pp)
https://doi.org/10.1088/1361-6463/ad6876

On the modes of nanosecond pulsed plasmas for combustion ignition of quiescent CH_4-air mixtures

Chunqi Jiang[1,2,*], Akash C Dhotre[4], Meimei Lai[1], Sayan Biswas[3,4], James R MacDonald[3] and Isaac W Ekoto[3,*]

[1] Frank Reidy Research Center for Bioelectrics, Old Dominion University, Norfolk, VA, United States of America
[2] Department of Electrical and Computer Engineering, Old Dominion University, Norfolk, VA, United States of America
[3] Sandia National Laboratories, Livermore, CA, United States of America
[4] Department of Mechanical Engineering, University of Minnesota, Minneapolis, MN, United States of America

E-mail: cjiang@odu.edu and iekoto@sandia.gov

Received 4 March 2024, revised 12 April 2024
Accepted for publication 29 July 2024
Published 6 August 2024

Abstract

The effect of transient plasma modes on ignition kernel development are discussed here for a quiescent CH_4-air combustion model system. A 10 ns high-voltage pulse was applied to a pin-to-pin electrode in lean fuel-air mixtures at room temperature and atmospheric pressure. High-impedance streamer, transient spark and low-impedance spark discharges were identified based on pulse waveforms of voltage and current. A sustained ignition kernel expansion was observed when the plasma discharge transitioned into a transient spark or spark discharge. The minimum ignition energy was obtained at the transient spark mode, which has less than a third of the energy or Coulomb transfer compared to the low-impedance spark. Employing repetitive 10-pulse sequence at 10 kHz, the lean-fuel limit was extended from an equivalence ratio of 0.6 for the single pulse ignition to 0.5. The use of repetitive pulses also allowed streamer breakdown or spark initiation to occur at a lower voltage.

Keywords: pulsed, plasmas, combustions, ignitions, quiescent, CH_4

1. Introduction

Economic and environmental concerns have motivated increasingly strict carbon dioxide (CO_2) and pollutant emission requirements for new passenger and commercial vehicles [1, 2]. In response, engine developers have sought new and novel technologies that both improve efficiency and reduce pollutant emissions for existing internal combustion (IC) engines and enable use of emerging renewably sourced combustion fuels such as hydrogen or alcohols for future IC engine architectures.

For spark ignited (SI) engines, the most effective pathway for fuel economy improvement is to introduce excess-air (*i.e.* lean-burn) or recirculated combustion products (*aka.,* exhaust gas recirculation (EGR)-dilute) into the oxidizer stream [3, 4]. These combustion strategies feature higher volumetric efficiencies that reduce part-load operation pumping losses, higher charge specific heat ratios that increase cycle thermodynamic efficiencies and lower combustion temperatures that reduce wall heat transfer. Lower combustion temperatures also reduce engine-out emission of nitrogen oxides (NO*x*) and particulate matter. Lean-burn and EGR-dilute engines are also well-matched to hybridized powertrain systems that enable

* Authors to whom any correspondence should be addressed.

extensive operation with the highest efficiency. Finally, most lean-burn and EGR-dilute combustion strategies work well with renewably sourced hydrogen or alcohols as SI fuels.

The critical challenge for lean-burn and EGR-dilute combustion strategies is to achieve stable ignition under dilute conditions where the initial flame kernel is more prone to extinguish due to lower flame speeds and higher sensitivity to strain. Conventional inductive spark ignition systems have limited effectiveness for these combustion strategies due to heat losses and confinement of the ignition kernel by the closely spaced sparkplug electrodes. Recently, use of high-tumble in-cylinder flows and wider gap sparkplugs has improved charge ignitability through elongation of the discharge with ignition kernel formation occurring away from the comparatively cooler electrodes [5, 6]. Larger initial ignition kernels are less likely to be quenched by electrode surfaces. However, this comes at the cost of higher head and piston surface heat transfer losses due to increased in-cylinder turbulence as well as accelerated igniter wear due to higher discharge voltage requirements.

A viable alternative is to use advanced igniters that generate larger and more distributed ignition volumes, with ignition duration extended through active management of ignition energy delivery. Challenges and advantages of various advanced ignition systems such as high-energy spark ignition, pulsed nanosecond discharge ignition, radio-frequency plasma ignition, laser-induced plasma ignition, and pre-chamber ignition have been discussed in recent reviews [7, 8]. Promising improvements over the conventional ignition systems have been demonstrated for many of these innovative ignition systems by extending lean-burn and dilution limits [7, 8]. Among them, arc-free, non-thermal plasma-based ignitors are generally more erosion resistant, with promise for low cost and energy consumption [8]. Low-temperature plasma-based technologies including transient plasma ignition (TPI) and other plasma-assisted combustion are hence of great interest to the advancement of IC engine technologies with high potential to enable lean or carbon-free fuel ignition with minimal energy requirements.

In the 1970s, Maly and Vogel [9, 10] identified the breakdown, arc, and glow modes of conventional spark discharges. The breakdown mode involved transient establishment of an electrically conductive channel between the anode and cathode during the first 1–10 ns of the discharge. An advantage of the transient breakdown mode was the superior energy deposition into the gas relative to the other modes with energy transfer efficiencies approaching 95% [9]. In the early 2000s, TPI, typically in the form of weakly-ionized streamers, was proposed as a pulsed detonation engine ignition source that could reduce ignition delay time and improved fuel economy [11, 12]. TPI uses short (e.g. <50 ns) high voltage pulses to initiate low-temperature plasmas in single-point or multipoint spark-plug systems, with larger ignition volumes and shorter ignition delays relative to conventional spark ignition [13, 14]. More recently it has been observed that high-frequency (>30 kHz) repetitive nanosecond pulses can enhance ignition kernel growth by increasing the ignition probability and kernel area through 'inter-pulse coupling' [15]. Repetitive nanosecond pulse sequences at 10 kHz have been shown to further reduce ignition delays relative to single-pulse ignition alone, which was found to increase the likelihood of successful ignition for lean and dilute fuel-air mixtures [16, 17].

Despite the progress made in the application of nanosecond pulsed plasmas for combustion system applications, fundamental understanding of the modes of plasma discharges and their impact on subsequent ignition processes is limited. Pai *et al* reported that for atmospheric pressure air preheated to 1000 K, nanosecond repetitively pulsed discharges can have different modes or regimes that include weakly ionized corona streamers and highly conductive spark channels [18]. Recent studies have shown that preceding weakly ionized discharge can impact subsequent discharge modes in the pulse sequence, and ultimately impact the energy deposition and lean-ignition limit [17, 19, 20].

It has been demonstrated previously that fuel-air mixtures at equivalence ratios (ϕ) close to stoichiometric, *i.e.* $\phi = 1.0$, were ignited with single or repetitive 10 ns pulsed discharges [17, 19]. However, ignition for the surface discharges was only observed when the discharge transitioned to a low-impedance spark characterized by extremely high pressures and temperatures from the high current flow and hence energy deposition into the gas. While effective for ignition, this type of discharge mode results in rapid erosion of electrode surfaces. For the present study, the influence of the discharge mode (i.e. streamer, transient spark, and filamentary spark) and pulse strategy (i.e. single- or multi-pulse) were evaluated for quiescent CH_4–air mixtures at atmospheric pressure with lean fuel ratios ($\phi = 0.5$–1.0) using a pin-to-pin electrode configuration. A unique mode of ns-pulsed discharge, transient spark, was identified and compared with other modes for lean fuel ignition. Time-resolved schlieren imaging was performed to analyze ignition kernel transition to a sustained flame. Time-resolved chamber pressure was also recorded to evaluate the combustion performance under different pulse strategies for various fuel ratios.

2. Experimental setup and methodology

Experiments were carried out in parallel for the same electrode configuration and pulsed power conditions using two separate high-pressure test rigs at Old Dominion University (ODU, Norfolk, VA) and the Combustion Research Facility located in Sandia National Laboratories (SNL, Livermore, CA). Both test rigs consist of a stainless-steel chamber, a pin-to-pin ignition electrode, a flow and pumping system, and a piezoresistive pressure transducer, as shown in figure 1(a). The ODU test chamber was assembled from a ConFlat® cube of 114.3 mm each side and has an internal volume of approximately 700 cm^3. Gas mixing and chamber pressure were controlled by the flow and pumping system that consisted of needle and toggle valves, a digital pressure gauge (McMaster, high-accuracy 2.1 bar pressure gauge) and a rotary vane vacuum pump (Alcatel 2008A). The SNL combustion apparatus has been discussed in detail previously [21]. The test

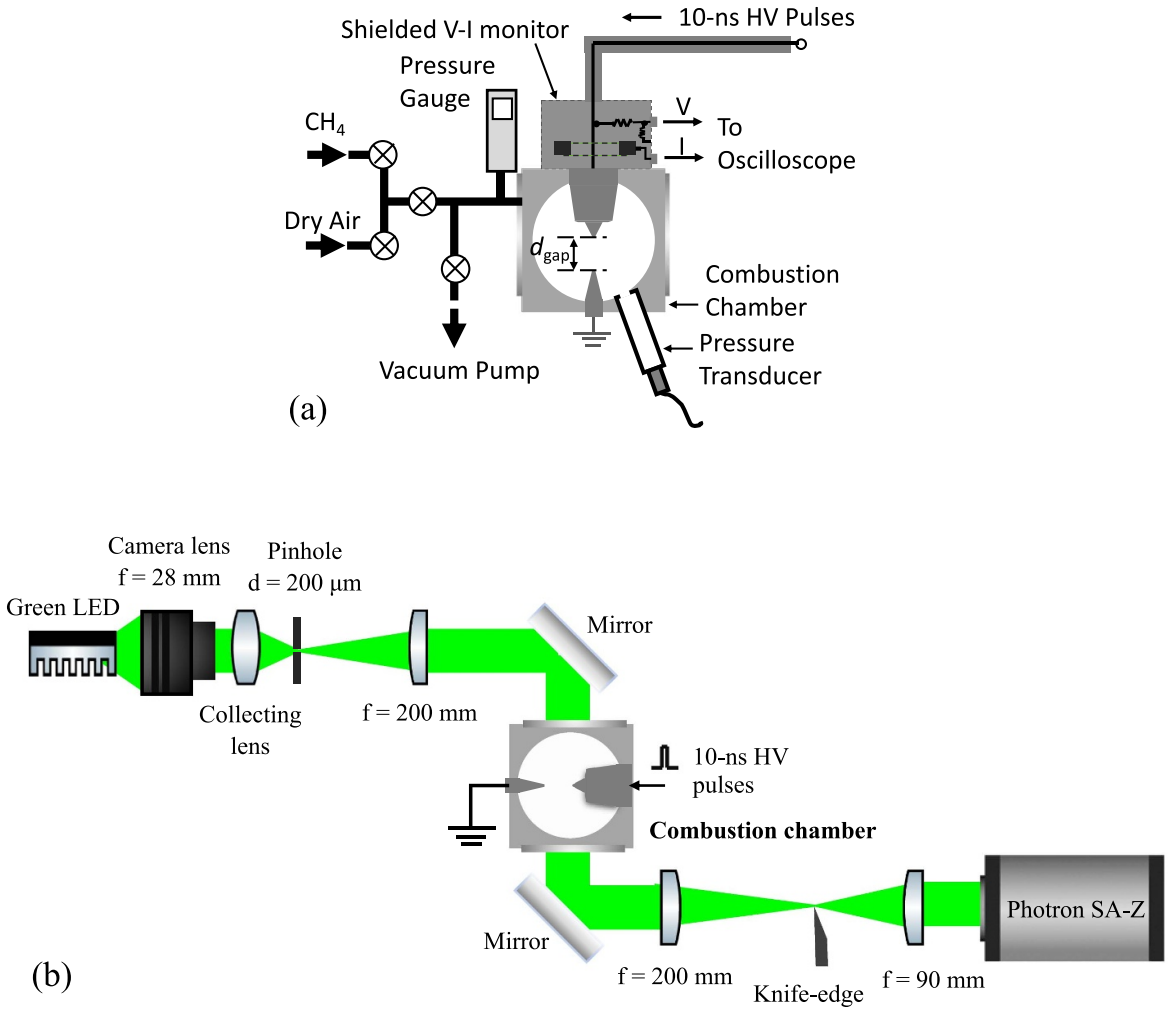

Figure 1. (a) Schematic of a static methane-air ignition testing system for the 10 ns transient plasma using a pin-to-pin electrode configuration, and (b) the corresponding optical schematic of schlieren imaging to visualize the transient plasma ignition for combustion.

chamber was equipped with UV-grade windows for schlieren imaging and has a total 29 cm^3 internal volume, which is significantly smaller than the ODU chamber.

The same electrode configuration was applied to both ODU and SNL chambers. The high voltage pin of the electrode system was made of a modified non-resistive sparkplug (Brisk MR12LS), mounted to the combustion chamber through an available port, as shown in figure 1(a). The tip of the sparkplug pin was rounded to a radius of 125 μm, with its J-hook and top 4 mm of the outer metallic body removed. A 3.18 mm diameter stainless steel rod that has a cone frustum with a 125 μm diameter tip, was used as the ground pin. It was connected to the chamber with a Swagelok fitting through the opposite port from the high voltage pin. Positive 10 ns high voltage pulses were provided by identical nanosecond pulsed power sources (Transient Plasma Systems (TPS) SSPG-20X-HP1).

For the ODU test rig, a custom-built *V–I* monitor was inserted between the high voltage coaxial cable from the power supply and the spark plug electrode for accurate voltage and current measurements. The *V–I* monitor [19, 22] consisted of a 20:1 voltage attenuator and 1 V/A current probe (Pearson 6585), and was connected to a high-speed digital oscilloscope (Tektronix DPO 5204) with 50 ohm coaxial cables, BNC attenuators and 50 ohm terminators. Built-in voltage attenuators were also equipped in both TPS pulsed power sources, allowing comparison of the experimental conditions and results between two teams. The high voltage nanosecond pulsed power source could produce up to 20 kV, 10 ns pulses into a 50 ohm load at repetition rates of up to 10 kHz. Delay generators (e.g. Stanford Research Systems, DG535) were used to provide trigger signals for the pulse generators. Ignition tests were carried out by initiating the pulsed discharges in static fuel-air mixtures with various ϕ. After evacuation, the chamber was filled with methane (Airgas, 99.5% methane) to a certain partial pressure, followed by dry air (Airgas, $<$7 ppm H_2O) to a total pressure of 1.0 bar. Each measurement was repeated at least three times. A static CH_4-air mixture may be initiated with a single high voltage pulse or a pulse train

containing multiple repetitive pulses. The required voltage amplitude and the lean limit of single and multiple pulse ignition schemes were investigated.

For the SNL test rig, gas mixing was achieved by adjusting mass flow controller (MKS GE50-DS) air and methane flow rates into a 1 l stainless steel sample cylinder that functioned as a mixing plenum, with the fuel-air mixture then sent to the ignition chamber at a specified ϕ and fixed pressure of 1 bar absolute. Similar voltage and current probes were positioned to monitor line voltage between the pulse generator and load with the probes located 66 cm before the igniter. All data were recorded using a LeCroy HDO 6054 500 MHz high-definition oscilloscope. Recorded pressures were filtered by a 1 kHz low-pass filter during post-processing to remove discharge generated noise.

Schlieren imaging of each ignition event was simultaneously performed using a Z-type configuration (figure 1(b)). Visualization into the chamber was allowed by two opposed UV-graded quartz windows that are installed into the chamber side walls—each with a16 mm outer diameter and 12.7 mm clear aperture. Light for the schlieren was achieved using a pulsed green light-emitting diode (LED) that was overdriven by a custom LED driver to produce intense, short pulse (<1 μs) light. A Nikkor 28 mm lens and condensing lens were used to collimate the LED light. Focusing optics and a knife edge were used to project the schlieren image directly onto the CCD array of a PhotronSA-Z high-speed camera. Schlieren images were recorded at 20 000 frames per second with 12 μs exposure times and were post-processed to remove noise and increase contrast.

3. Results

3.1. Single-pulse ignition of fuel-air mixtures

3.1.1. Modes of the transient plasma. Figure 2 shows the voltage and current waveforms of the transient plasma under different discharge modes driven by a single pulse. When the pulsed voltage is relatively low, the discharge manifests as a weakly ionized streamer. As shown in figure 2(a), the presence of a shoulder pulse after the main 10 ns voltage pulse extends the full-width-half-maximum (FWHM) to be 13 ns and indicates that the circuit is overmatched due to the relatively high impedance of the plasma. A highly transient current pulse with a FWHM of 4.5 ns occurs during the voltage pulse and has a maximum of 57 A. At the weakly ionized streamer mode, no successful ignition for combustion was observed. Integrating the current or the product of the voltage and current over a sufficient time, e.g. 1500 ns, the Coulomb transfer or energy per pulse was obtained, respectively. The energy per pulse at the high-impedance mode was calculated to be 2.0–2.5 mJ for the pin-to-pin system in one atmosphere air for the voltage of 8–9 kV. The Coulomb transfer is negligible at this mode, in the range of tens of nF.

At a higher voltage, e.g. 9.3 kV, the discharge transitioned from a streamer to a transient spark, as shown in figure 2(b). The transient spark, *aka*. abnormal glow, emerges during the falling phase of the voltage pulse and is represented by a current pulse with a duration of 18 ns. It follows a typical current pulse, about 4 ns duration, for a streamer discharge (figure 2(a)). The energy per pulse and Coulomb transfer for the first group of pulses including both streamer and transient spark are 4.3 mJ and 1 μC. The remanent charge accumulated in the system may result in a second transient spark discharge or a 'soft' breakdown under excitation of a small ($<$500 V) voltage pulse due to the reflection of the pulse generator circuit (figure 2(b)). This soft breakdown contributes to significantly more charge transfer (8 μC) but only a small energy deposition (0.1 mJ), resulting in a total energy per pulse of 4.4 mJ and Coulomb transfer of 9 μC.

When voltage was increased above 12 kV, the streamer transitioned to a filamentary spark discharge with peak current $>$150 A and an elongated decay time, as shown in figure 2(c). Decay time—defined as the duration for 90%–10% peak value—was 0.4 μs for the hard breakdown excited by a 13 kV pulse, which is $>$3 times that of a transient spark. The energy per pulse and Coulomb transfer were calculated to be 11 mJ and 30 μC. The minimum energy per pulse and voltage to reach the filamentary spark mode were found through testing to be 8 mJ and 12.2 kV respectively.

Since the transient spark mode (together with the soft breakdown) achieved successful ignition using less energy than the high impedance spark alone, the minimum ignition energy (MIE) was hence obtained for the transient spark mode, which for single-pulse ignition was determined to be 4 mJ for a very lean fuel-air mixture of $\phi = 0.6$ at a voltage of 9.3 kV.

3.1.2. Ignition kernel development with single pulse excitation. Ignition kernel development and subsequent flame propagation can be observed via a sequence of schlieren images in figure 3. Four exemplar schlieren image sequences taken in the region centered at the pin-to-pin electrodes in the SNL chamber for single-shot plasma ignitions at a close to stoichiometric equivalence ratio, $\phi = 0.8$ (figures 3(a)–(c)), and at a lean mixture ratio, $\phi = 0.6$ (figure 3(d)) are provided. For the schlieren images, pulsed voltages of 12.4–13.5 kV were applied to the electrodes. The first image of each sequence was synchronized to time of discharge voltage, which corresponds to $t = 0$.

Figure 3(a) is a sequence for a failed ignition. No discharge was observed in the first image of the sequence, likely due to insufficient sensitivity of the schlieren diagnostic, which suggests the discharge remained a weakly ionized streamer. The schlieren diagnostic detects index refraction gradients that result from an increase in gas temperature, but weakly ionized streamers only produce low amounts of heat from relaxation of excited vibrational or electronic states. By 0.05 ms after the discharge a bifurcated streamer channel was plainly visible as slower vibrational relaxation processes provide sufficient heat for the streamer channel to be visualized by the schlieren diagnostic. The streamer remained visible out to 0.6 ms after the discharge, but no evidence of the ignition kernel formation was observed.

The ignition image sequence in figure 3(b) is of a transient spark that initiated a diffuse ignition kernel, which asymmetrically grew into a successful ignition. An asymmetric growth

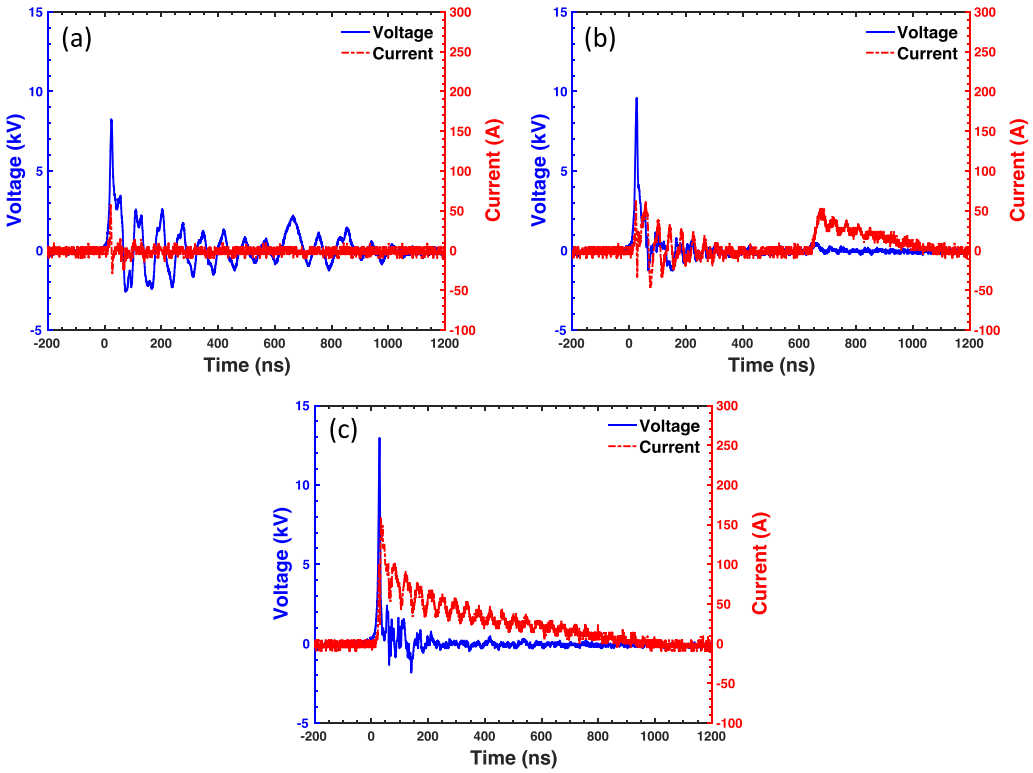

Figure 2. Typical voltage and current waveforms of nanosecond HV pulses across the pin-to-pin electrode in a static CH_4-air mixture with an equivalence ratio ϕ of 0.8 at 1 bar when the discharge is at (a) a high impedance mode when no breakdown occurs, (b) a transition mode when a transient spark discharge follows the initial streamer and a soft breakdown is initiated by a reflected voltage pulse, and (c) a low-impedance spark discharge mode and breakdown is initiated by the main voltage pulse.

of the flame kernel is characterized by that the combustion flame propagates only in a certain direction and diminishes in the other. Conversely, the ignition image sequence from figure 3(c) is of a filamentary spark produced from a hard breakdown—evidenced by the bright light emission observed at $t = 0$—that led to a symmetric ignition kernel. Note that the symmetric growth of the flame kernel is only approximate. Also note that relative to the transient spark ignition in figure 3(b) (with the energy per pulse in the range of 5–7 mJ), the filamentary spark ignition in figure 3(c) exhibited stronger early kernel growth in the radial direction likely due to more discharge energy, about 20–30 mJ. For the leanest condition ($\phi = 0.6$) ignition sequence shown in figure 3(d), a filamentary spark discharge was initiated by a 12.4 kV pulse that was followed by a symmetric ignition kernel similar to what was observed in figure 3(c). No successful ignition was observed for $\phi < 0.6$ with only a single pulse.

3.1.3. Combustion performance with single pulse ignition. To evaluate combustion performance within the chamber, peak pressure (P_{peak}), i.e. the maximal pressure reached in the given combustion vessel, and ignition delay (t_d), i.e. the time needed to reach 10% of the maximal pressure since the application of the pulsing, were measured. Figure 4(a) includes exemplar pressure traces during combustion for CH_4/air mixtures at $\phi = 0.8$ and 0.6, recorded from the SNL chamber. Note that trigger noise at the beginning of the pressure trace was from the nanosecond voltage pulse, and its onset was used to indicate the start time, $t = 0$. Pressure traces in figure 4(a) for $\phi = 0.8$ correspond to the ignition sequences from figure 3(b) (transient spark: blue) and 3(c) (filamentary spark: red). Filamentary spark ignition led to a symmetric ignition kernel growth, which resulted in a shorter ignition delay but lower P_{peak} relative to the asymmetric kernel growth from a transient spark ignition.

Ignition delay (t_d) values are plotted along with the peak chamber pressure (P_{peak}) in figure 4(b) as a function of ϕ using the ODU chamber. Each condition was repeated 3–10 times, and the error bars represent the range of values observed. Figure 4(b) shows that the peak pressure decreases, and the delay time increases with ϕ decreasing. Additionally, the difference in ignition mode likely contributed to the observed variation in ignition delay and peak pressure, with these variations increasing with a decrease in ϕ. Note that regardless of ϕ, no significant impact on discharge breakdown criteria or mode transition between streamer, transient spark, and filamentary spark discharge was observed. The minimum ϕ allowing successful combustion was found to be 0.6 under the single-shot ignition condition.

3.2. Multi-pulse ignition of lean fuel-air mixtures

3.2.1. Voltage, current and energy of a repetitive multi-pulse ignition. An example pulse train consisting of 10 pulses with a pulse repetition frequency (PRF) of 10 kHz, used to ignite a lean CH_4-air mixture ($\phi = 0.5$), is shown in figure 5.

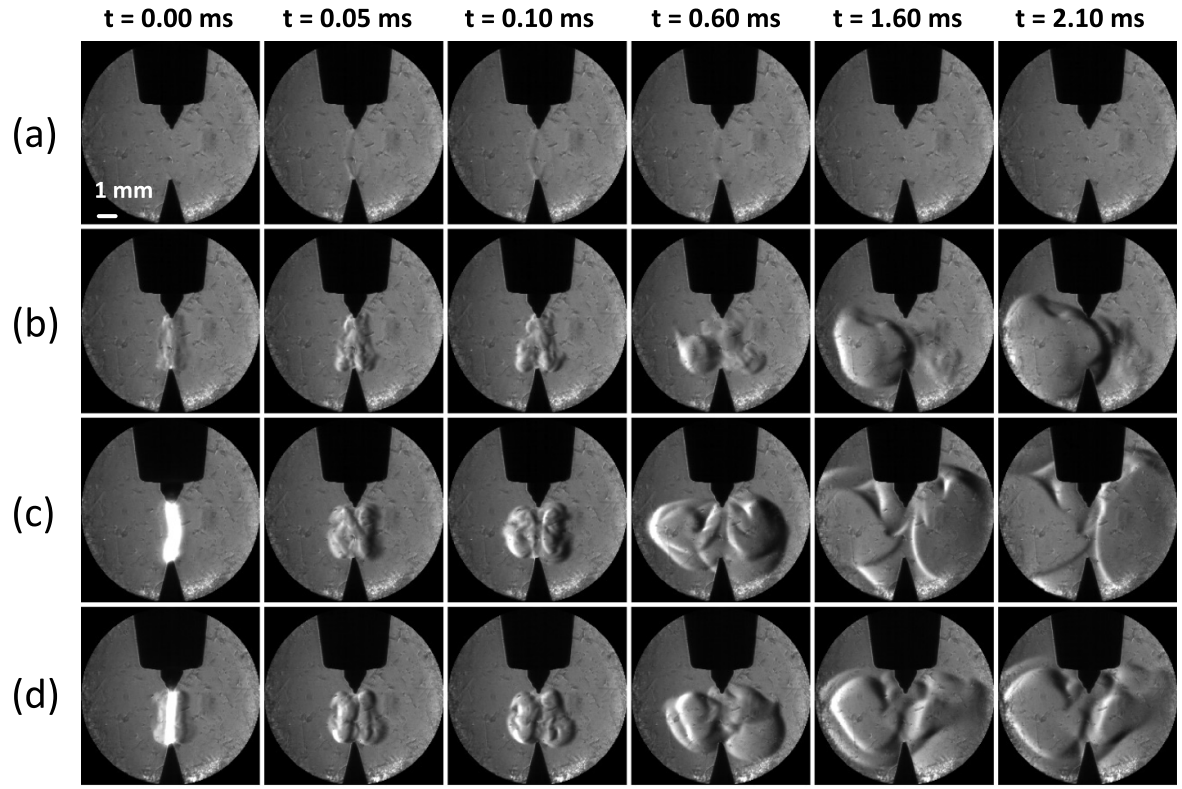

Figure 3. Schlieren images of the temporal development of the TPI for combustion after applying a single voltage pulse at $t = 0$ to the static CH_4-air mixture at $\phi = 0.8$: (a) a high-impedance streamer discharge with no ignition kernel development, (b) a transient spark with breakdown occurring after the main voltage and during the reflected pulse that resulted in a successful ignition, but with asymmetric kernel growth, (c) a filamentary spark with complete breakdown during the main voltage pulse that resulted in successful ignition with a symmetric flame kernel, and (d) a filamentary spark that produced a symmetric flame kernel and led to successful ignition for a $\phi = 0.6$ mixture.

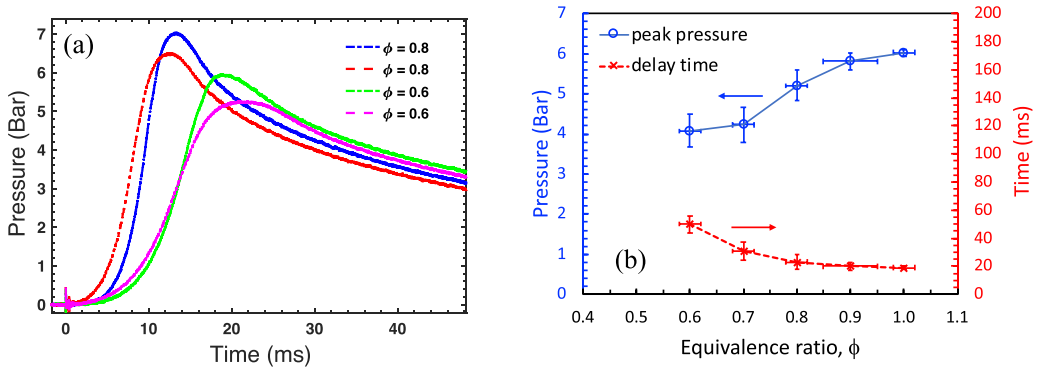

Figure 4. (a) Pressure traces of combustion initiated a single pulse, obtained in the SNL chamber filled with static CH_4/air mixtures with equivalence ratios, $\phi = 0.8$ and 0.6, using the SNL chamber, and (b) the peak pressure and ignition delay with respect to the equivalence ratio for the single-shot plasma ignition obtained in the ODU chamber.

Figure 5(a) is a plot of voltage and current waveforms as a function of time during the entire sequence. Figure 5(b) is a zoomed-in plot of the voltage and current waveforms for the 1st pulse when a 10 ns, 7.8 kV pulse initiated a high-impedance streamer discharge. The 2nd pulse (not shown) qualitatively resembles the 1st one. A hard breakdown associated with a low-impedance filamentary spark discharge occurred during the 3rd pulse, as shown in figure 5(c), and the remaining pulses in the sequence all resemble this pulse. Finally, discharge energy and Coulomb transfer for each pulse in the sequence are plotted in figure 5(d), with values ranging from 1.5 mJ and ∼0.1 μC for the first two pulses at the high-impedance streamer mode to ∼5 mJ and 10–35 μC for the rest of the low-impedance, spark-discharge mode pulses. The total energy and Coulomb transfer of the 10-pulse sequence were 40 mJ and 210 μC, respectively. The discharge mode transition from a high-impedance streamer to a low-impedance spark can be clearly observed by the jump in pulse energy as well as the increase in Coulomb transfer. When operated under multi-pulse at 10 kHz, hard breakdown was observed at ∼8 kV.

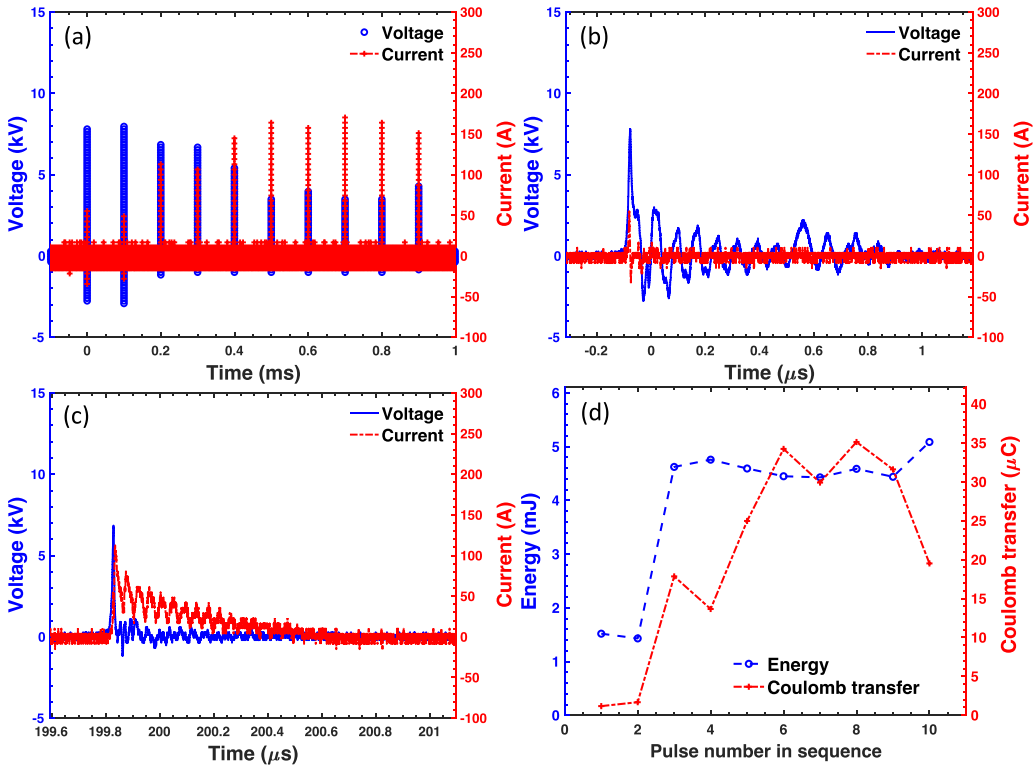

Figure 5. Voltage and current waveforms of a pulse sequence containing 10 pulses at 10 kHz that were used to ignite a static CH_4-air mixture of $\phi = 0.5$ at 1.0 bar for: (a) the entire pulse sequence, (b) the first pulse in the sequence that featured a high-impedance discharge without breakdown, (c) the third pulse in the sequence with a low-impedance spark discharge due to breakdown initiation, and (d) the energy and Coulomb transfer for each pulse. The remaining pulses in the train all resemble the low-impedance spark discharge shown in (c).

Depending on the voltage applied and given the stochastic nature of the breakdown process, the low-impedance spark discharge or transient spark was observed to be initiated as early as the first pulse and as late as the last one. Importantly, applying multiple pulses at a relatively high PRF (e.g. >5 kHz) allowed breakdown to occur at a much lower voltage. Similar phenomenon due to the memory effect of the proceeding discharges on the breakdown voltage was reported and discussed in details previously [19, 23]. The lower breakdown voltage for the low impedance spark resulted in lower energy deposition in the discharge. Multiple repeated measurements for voltages ranging from 8 to 10 kV were tested for the multi-pulse ignition at various fuel-air mixture ratios. While the energy per pulse for a high-impedance streamer is consistently less than 2 mJ, it was in the range of 5–7 mJ from both transient and low-impedance spark modes, with no significant difference between the two spark modes. However, the Coulomb transfer during the low impedance spark is consistently higher, up to 40–50 μC, compared to 10 μC or lower for the transient spark.

3.2.2. Ignition kernel development with multi-pulse ignition. Ignition sequence images in figure 6 are of the discharge, ignition kernel development, and subsequent flame propagation for stoichiometric ($\phi = 1.0$) and lean ($\phi = 0.6$ and 0.55) CH_4-air mixtures as a result of 5- or 10-pulse trains with fixed 10 kHz PRF and peak pulse voltages between 8.2–8.8 kV. The first frame of each image sequence (i.e. column) corresponds to $t = 0$, when the first pulse was applied. In each case, visual evidence of a discharge streamer or ignition kernel was visible. The 3rd frame of each image sequence shows a breakdown (either a transient spark accompanied with soft breakdown or a low-impedance spark discharge) that led to ignition. Note that the frame rate of the ICCD camera is 20 kHz, which allows two frames per pulse in a pulse sequence of 10 kHz. The image sequence in figure 6(a) is from a $\phi = 1.0$ mixture with an 8.2 kV, 10-pulse train. From the sequence, no discernible evidence of the discharge was visually observed until the 7th pulse (i.e. 0.6 ms). A bright filamentary spark discharge overlaid the ignition kernel during the 10th pulse, as shown in the 3rd frame of figure 6(a), which was followed by successful kernel development, growing in a toroidal shape, as shown in the rest frames of figure 6(a). The discharge current was not measured directly during the Schlieren imaging. Based on the systematic power measurements obtained separately for similar voltage and modes of discharge, the total energy in the plasma was estimated to be <40 mJ. The fact that the pulse voltage was well below the 12.2 kV thresholds required to produce a low-impedance spark for a single-pulse discharge suggests the memory effect induced by the preceding weakly ionized streamers facilitated this transition. Once the ignition kernel is established successfully, the following pulses may not be needed. A similar image sequence from a successful ignition of a $\phi = 1.0$ mixture with only 5 pulses is provided in figure 6(b). During the 5-pulse ignition, a low-impedance spark was achieved on the final pulse in the sequence (i.e.

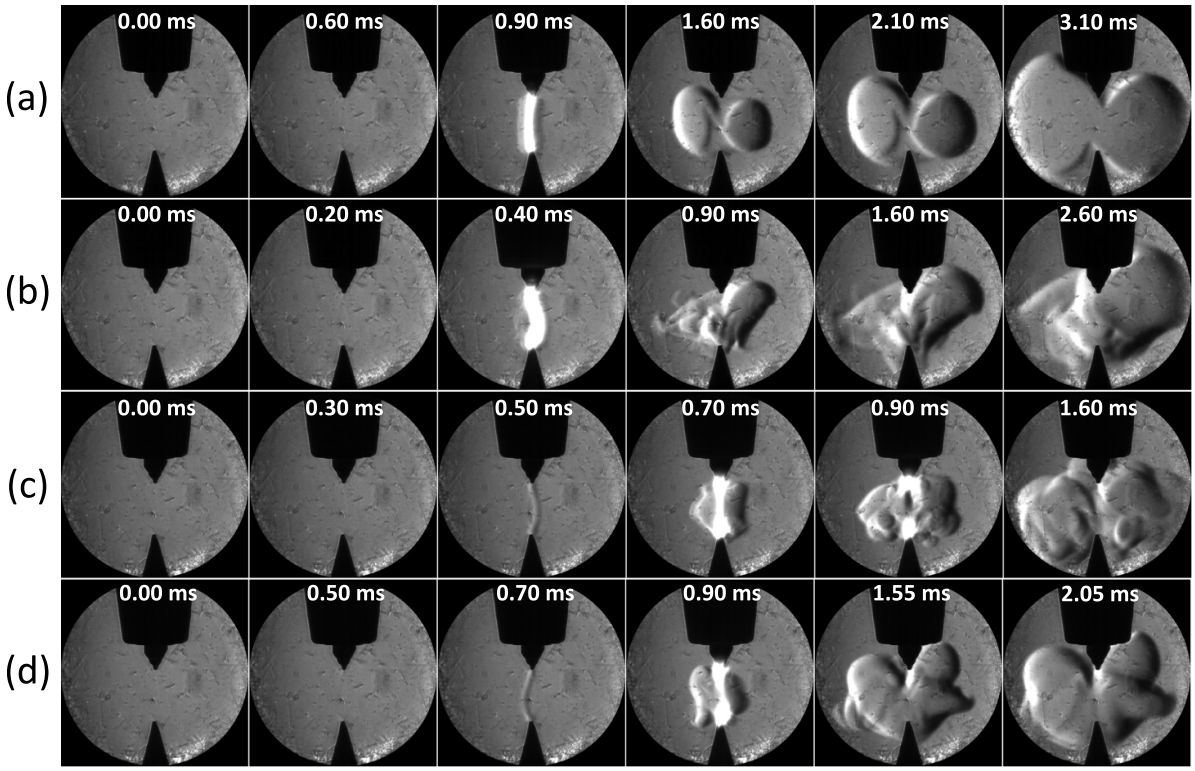

Figure 6. Schlieren images of the temporal development of the ignition kernel after applying a sequence of pulses at 10 kHz to the quiescent CH_4-air mixture at one atmosphere: (a) a 10-pulse sequence for a stoichiometric mixture ($\phi = 1.0$), (b) a sequence of 5 pulses igniting a stoichiometric mixture ($\phi = 1.0$), and a sequence of 10 pulses igniting a lean mixture for (c) $\phi = 0.6$ and (d) $\phi = 0.55$ mixtures.

0.4 ms). The total energy deposition in the plasma was estimated to be ∼20 mJ. The spark channel was somewhat irregular as evidenced by the prominent bend in the lower portion of the discharge, and the associated flame kernel was likewise asymmetric.

Similar ignition sequences are provided in figures 6(c) and (d) for lean mixtures ($\phi = 0.6$ and $\phi = 0.55$ respectively). Each ignition event featured a 10-pulse train at 10 kHz. Unlike the stoichiometric ignition conditions, the first visual evidence of a lower intensity transient spark was observed in the 6th pulse (i.e. 0.5 ms) for $\phi = 0.6$ and the 8th pulse (i.e. 0.7 ms) for $\phi = 0.55$, with ignition observed thereafter. Because there were still remaining sparks in the 10-discharge pulse train, each additional discharge was observed to produce a low-impedance spark characterized by the highly luminous discharge channel that was completely contained within the burned gas region as the gas density was much lower in the burned gases relative to the unburned gases. The total energy deposition in the plasma was estimated to be ∼40 mJ for both figures 6(c) and (d). The additional pulses led to highly wrinkled flame fronts and faster than expected growth of the flame kernel with early kernel growth rates observed to be roughly as fast as they were for the stoichiometric mixtures despite the leaner mixtures having much lower flame speeds.

3.2.3. Combustion performance with multi-pulse ignition. Measured pressure traces from the SNL chamber for the multi-pulse ignition sequences from figure 6 are plotted in figure 7(a). For the stoichiometric 10-pulse (blue) and 5-pulse (red) ignition events, the initial portion of the pressure rise was almost indistinguishable out to around 9 ms. The result is somewhat surprising given that the kernel flame front with 10-pulse ignition was laminar whereas the kernel flame front with 5-pulse ignition was modestly wrinkled and thus had a higher flame surface area—and hence flame front velocity. Moreover, the 10-pulse ignition kernel was established a full 0.5 ms later relative to the 5-pulse ignition kernel. However, these advantages appear to have been offset by the asymmetric nature of the flame kernel for the 5-pulse ignition that led to less efficient volumetric utilization of available fuel in the chamber. Finally, it is notable that pressure-rise for the lean mixtures closely overlapped the stoichiometric mixtures for the first 2–3 ms. These results confirm the visual observation that a combination of flame front wrinkling and deposited pulse energy into the kernel enhanced kernel growth such that a stable flame was more likely to be established. As a result, the lean limit was extended from $\phi = 0.6$ for single pulse ignition to $\phi = 0.55$ for multi-pulse ignition.

Multi-pulse ignition experiments were also conducted in the ODU chamber to evaluate the trends of ignition delay

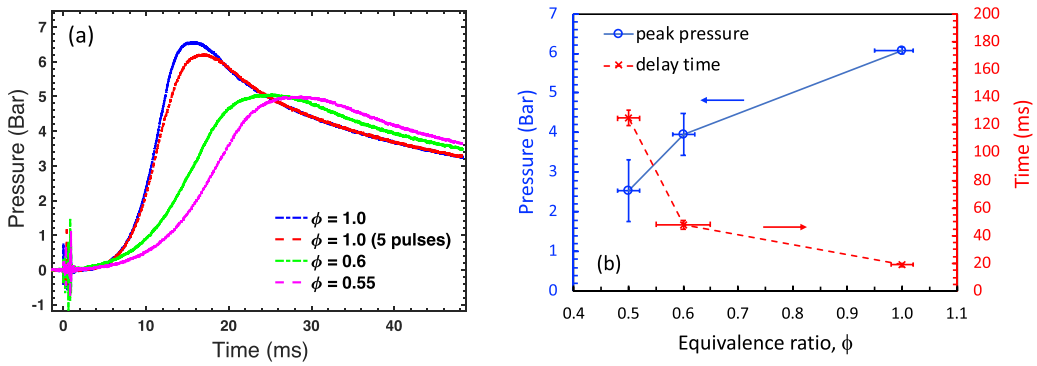

Figure 7. (a) Corresponding pressure traces (for figure 6) that resulted from ignition in the SNL chamber; and (b) the peak pressure and ignition delay obtained during combustion in the ODU chamber for ϕ ranging from 1.0 to 0.5. Except one case noted in (a), where only 5 pulses were applied, each ignition was accomplished by applying a 10-pulse sequence at 10 kHz for the fuel-air mixture at an initial pressure of 1.0 bar at room temperature.

and P_{peak} for ϕ values of 1.0, 0.6, and 0.5. At each condition, more than 3 repeated measurements were performed to assess repeatability. To achieve reliable ignition in extreme lean conditions, higher ignition energy is needed, which can be achieved by applying higher voltages for the same discharge mode. The pulse voltage of 10 kV was used here for all pulse sequences. Figure 7(b) shows that the P_{peak} and delay time at $\phi = 1.0$ and 0.6 obtained with 10-pulse sequences at 10 kHz are the same as those using the single-shot pulsed ignition (figure 4(b)). Importantly, multi-pulse ignition enabled successful ignitions at a leaner mixture ratio of $\phi = 0.5$, which is essentially the lean flammability limit for CH_4-air mixtures. Successful ignition for $\phi = 0.5$ mixtures was also obtained with 10-pulse trains when the PRF was lowered to 5 kHz, below which successful ignition was not achieved.

4. Discussion

4.1. Modes of discharge and their relations to ignition for combustion

The transient plasma for combustion ignition is typically referred to as weakly ionized corona or streamer discharges, which are excited by strong reduced electric fields, *E/n*, on the order of hundreds of Td [11, 13]. Here, *E* is the electric field strength and *n* is the number density of the gas. In atmospheric pressure air-fuel mixtures, electron impact dissociation of gas molecules and electron impact excitation of N_2 electronic states followed by quenching and molecular dissociation are the primary mechanisms contributing to radical productions by TPI [13, 24]. At moderate *E/n* (e.g. 50–100 Td), the radicals produced by streamers alone are not sufficient to sustain the ignition kernel, as shown in this study with single pulse excitation using the pin-to-pin electrode configuration (similar to a conventional J-plug). A more conductive mode, such as a transient spark or filamentary spark is required to form a sustainable ignition kernel that results in a successful ignition.

The transient spark (as shown in the first group of pulses in figure 2(b)) is an abnormal glow discharge that occurs prior to breakdown. The current pulse is on the order of tens of ns, which is 4–5 times longer than a pulsed streamer but an order of magnitude shorter than a low-impedance spark. The transient spark starts with a high-impedance streamer characterized by the establishment of a relatively high *E/n* that in turn leads to an electron avalanche process in the streamer wake. However, the short duration of the voltage pulse leads to abrupt elimination of the external electric field and hence rapid quench of the avalanche process. Importantly, increased ionization rates during this mode facilitated radical production and provided remnant charge for follow-on pulses either from circuit pulse reflections or from subsequent pulses.

It is evident that pulsed streamer breakdown plays an important role in the plasma ignition process. Breakdown typically refers to the formation of a highly conductive discharge channel in the form of an arc-like discharge, which is represented by a collapse of the voltage and sharp increase in current as shown in figure 2(b) (soft breakdown), figures 2(c) and 5(c) (hard breakdown). During the highly conductive spark discharge, if the plasma impedance stays mostly constant, the decay of the discharge current can be fitted with a time constant τ after reaching its maximum when the voltage collapses to nearly zero. The electrode system can be simplified as a *RLC* circuit, where a small inductance *L* of the electrode is in series with a *RC*-parallel circuit. The series inductance includes all the circuit inductance of the high voltage connector and electrodes. The parallel circuit consists of a resistance *R* of the transient plasma and the electrode capacitance *C*. The capacitance of the interelectrode gap is negligible compared to the measured 24 pF capacitance of the sparkplug. The current waveforms of the breakdown/spark discharge shown in figures 2(b), (c) and 5(c) demonstrate underdamped responses, where the damped frequency of the current decay can be approximated by the natural frequency,

$$\omega_0 = \frac{1}{\sqrt{LC}}, \tag{1}$$

assuming the damping factor $\ll 1$, and the time constant can be depicted as

$$\tau = RC. \tag{2}$$

An underdamped current response $I(t)$ of a *RLC* circuit can be generalized as

$$I(t) = I_0 e^{-t'/\tau} \cos(\omega_0 t + \varphi), \quad (3)$$

where I_0 is the initial current at $t' = 0$ or the peak current before decay, and φ is the initial phase. Note that we use t' here for the underdamped response and to differentiate it from the time t of the whole ignition event. Applying Equ. (3) to fit the decay segment of the spark discharge current (e.g. as shown in figures 2(b), (c) and 5(c)), we found $\tau = 0.25 \pm 0.02$ μs and $\omega_0 = 0.145 \pm 0.005$ GHz for all breakdown cases. Based on these results, the damping factor is $\sim$0.02, which is reasonably small and agrees with our assumption. Using $C = 24$ pF, equations (1) and (2), we obtain the circuit inductance and plasma resistance to be 2 μH and 10.4 kΩ, respectively. Interestingly, although the spark discharge from the soft breakdown was initiated with a much lower voltage (e.g. $<$1 kV) compared to that from the hard breakdown, the plasma resistance is the same. Since the resistance/conductance of the plasma can ultimately be related to the plasma density and temperature, it shows that both the soft and hard breakdown obtain the same discharge mode.

The highly conductive spark discharge mode is distinctly different from either the transient spark or streamer mode, where the plasma is relatively weakly ionized, and the high-impedance of the plasma load results in the overmatched response to the incoming 10 ns pulses. Compared with spark discharges, in addition to the difference in plasma impedance, streamer or transient discharges have negligible or less Coulomb transfer and less energy delivery, which are important factors for combustion ignition applications. For this study, streamer discharge was not able to initiate a sustainable ignition kernel, as demonstrated in figure 3(a), and the transient spark or spark modes were necessary conditions to achieve successful ignition. Sufficient energy deposition in the ignition system was necessary to ensure sustained development of the ignition kernel without flame quench and to generate sufficient radicals to overcome losses with exothermic reactions. On the other hand, the use of very high voltage can induce highly energetic electrons that cause erosion at the electrode surface via sputtering. Excessively high Coulomb transfer that is associated with high ($>$13 kV) voltage-initiated spark during each ignition event can negatively impact the lifetime of the sparkplug electrodes. It is hence advantageous to obtain breakdown with lower voltages, such as the use of transient sparks or repetitively pulsed transient plasmas, to achieve reliable and energy-efficient ignition. For the single-pulse ignition event, the spark discharge achieved with soft breakdown requires lower (minimum 9 kV) voltage input and uses one third or less of the energy and Coulomb transfer, comparing to the hard breakdown which requires at least 12 kV. Both the ignition kernel propagation, shown in the schlieren images, and the following pressure development demonstrate that there is no significant difference in the pressure performance when the ignition is achieved by soft or hard breakdown or using higher or lower voltages to do so. As the soft breakdown essentially used a two-pulse sequence with a lower voltage pulse appearing 0.6 μs after the first main pulse, it is expected to see that breakdown can be achieved at a lower voltage using repetitive pulses. In fact, both soft and hard breakdown were obtained using a 10-pulse sequence at 10 kHz, 8 kV.

4.2. Repetitive multi-pulsed plasma ignition for lean burn

Relative to single-pulse discharge, repetitively pulsed discharge both lowered the voltage required and extended the lean limit for successful ignition. To understand why, it is useful to compare two successful ignition kernel development scenarios for a $\phi = 0.6$ mixture with either single-pulse (12.4 kV) or multi-pulse (10 kHz, 8 kV) discharge. Ignition kernel boundaries in both the left and right transverse directions with respect to the electrode axis were identified by subtracting two subsequent images. These images were then binarized using an adaptive function in MATLAB with high and low threshold pixel intensity values used to account for the light and dark sides of images respectively. An edge detection MATLAB function that calculates image gradient from the derivative of a Gaussian filter, was used to identify edges in the binarized image and hence to estimate the distance covered by the boundary in one timestep. While the flame boundary was somewhat sensitive to the thresholds selected or the schlieren image contrast ratio, the impact on displacement was negligible as the bias was in the same direction. The temporal displacement between frames was used to calculate transversal velocities of the kernel flames. Figure 8 shows the kernel velocity with respect to time for a single-pulse and a multi-pulse discharge in both the left and right directions. The first pulse of the 10-pulse sequence was applied at $t = 0$. Note that the first velocity data was obtained based on the first two frames of the kernel, and for multi-pulse the visible kernel imaging started at 0.7 ms due as the initial ignition kernel was not formed until the 8th pulse (i.e. $t = 0.7$ ms).

After the discharge, the initial transversal kernel boundary velocities for single-pulse ignition were 1 m s^{-1}. The velocity then increased slightly to 1.5 m s^{-1} within the first 2 ms and slowed down afterwards to 1 m s^{-1}by 4 ms as ignition transitioned to a sustained flame front. By contrast, initial kernel boundary velocities for multi-pulse ignition were initially 7.5 m s^{-1} at 0.8 ms, but rapidly decayed to around 2 m s^{-1} within 0.6 ms. No velocity data is available beyond 1.4 ms after the first discharge as the flame boundary had spanned the field of view. Because the multi-pulse discharge ignition kernel was able to grow rapidly, it was less sensitive to flame quench at the electrodes or localized extinction along the flame front. Accordingly, if the ignition kernel transitioned quickly enough into a fully developed flame using multiple discharges, successful ignition should be possible all the way down to the lower flammability limit, which is what was observed in the present study.

To explain why flame enhancement occurred with multi-pulse but not with single-pulse discharge, it is necessary to consider energy deposition into the kernel by successive discharges after the intimal flame kernel is established. To generate a first-order estimate of how energy deposition into the flame kernel would impact growth rates, the following

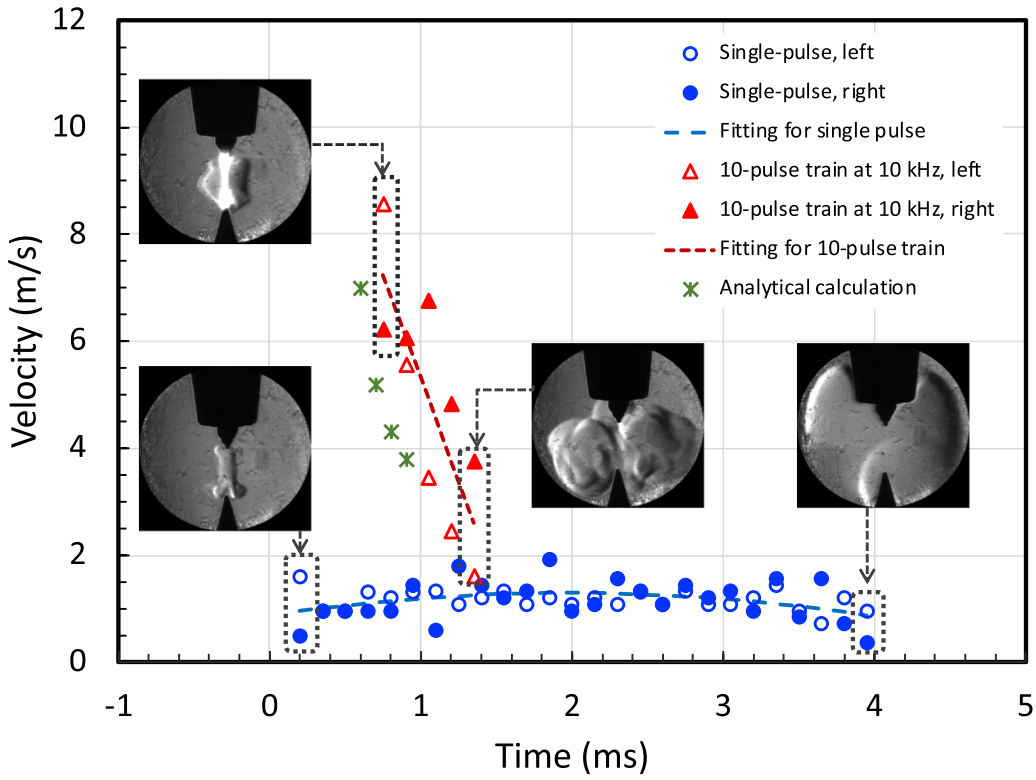

Figure 8. Temporal development of the transversal ignition kernel velocities for single-pulse (12.4 kV) and multi-pulse (10 pulses at 8.8 kV at 10 kHz) plasma discharges for a $\phi = 0.6$ mixture. A 2nd order polynomial fitting was applied to the average of the left and right velocities for the single pulse ignition, and a linear fitting was applied to the averaged multi-pulse ignited kernel velocities. The picture inserts were the schlieren images at the beginning and end of the kernel development for each case.

assumptions were made for the early growth period of the flame kernel:

1. The discharge energy was dissipated into the kernel as heat and the heat loss through the electrode surface was negligible during this period.
2. The change in chamber gas pressure during this period was negligible.
3. The ignition kernel was assumed to be an ellipsoid with the major axis aligned along the electrode axial axis and fixed at the 3 mm electrode gap distance. The minor axes were identical length and grew uniformly in the radial direction.
4. Heating of the ignition kernel from the discharge energy deposition was uniform, which in turn led to an isentropic expansion of kernel volume that was complete before the next pulse.

It is known that there would be heterogeneity in the temperature distribution [25] and the heating from the discharge is likely not limited to the unburned gas region. Assumption 4 hence may not be accurate. However, temperature inhomogeneity does not greatly impact on the isentropic kernel expansion, and as noted earlier the spark discharge was contained within the unburned gases and thus most gas heating was contained within this region. Thus, to first order, the assumption is reasonable.

Using the above assumptions, the increase in kernel temperature, ΔT, was approximately related to discharge energy, E_d, the number of moles within the kernel volume, n_{ign}, and the burned gas specific heat, $C_{p,b}$, as follows:

$$\Delta T \approx \frac{E_d}{n_{ign} C_{p,b}}. \tag{4}$$

Here, E_d, was assumed to be 5 mJ based on the measurements of low-impedance spark energy for the same gas and electrical conditions, while $C_{p,b}$ was calculated from the burned gas temperature prior to discharge and n_{ign} was calculated form the ideal gas law using the assumed ellipsoid ignition volume. Flame front displacement due to volumetric expansion was equivalent to half the growth of the minor axis, with the associated expansion velocity, U_{vol}, calculated by dividing the radial displacement by the interpulse dwell time (i.e. 0.1 ms). Kernel growth due to flame front propagation, U_{flame}, must also be considered, and was assumed to equal the 1 m s^{-1} measured for the early kernel growth period with single-pulse ignition. Total kernel front velocity, U, was accordingly approximated as the summation of the expansion velocity and the flame front velocity (i.e. $U = U_{\text{flame}} + U_{\text{vol}}$). Finally, the process was repeated for each successive low-impedance spark discharge but using the updated kernel volume boundary and temperature.

Estimated kernel front velocities calculated following the procedure outlined above are plotted in figure 8 for the 4 low-impedance spark events (i.e. at 0.6, 0.7, 0.8, and 0.9 ms) that occurred after the flame kernel was established at 0.5 ms.

The predicted value of 7 m s^{-1} for the first low-impedance spark is around 0.5 m s^{-1} slower than the mean of the leftward and rightward propagating front. The result suggests that thermal expansion from deposited discharge energy largely drove the rapid increase in kernel volume at this early stage. The 2nd, 3rd, and 4th pulses have predicted expansion velocities of 5.2, 4.3, and 3.8 m s^{-1} respectively that are roughly 1 m s^{-1} below the respective measured means of the leftward and rightward propagating front. Thus, while the trends are well matched, these results suggest additional physics are in play. The largest impact not captured in the simplified model is likely enhanced turbulence at the flame front due to large hydrodynamic forces generated by the discharge. Increased radical formation and burned gas temperatures from the discharge also likely contributed to faster propagation velocities [20, 26].

When pulse number was decreased from 10 to 5 with the PRF fixed at 10 kHz or if the PRF was reduced to 5 kHz with pulse number fixed at 10 pulses, successful ignition was still observed at $\phi = 0.5$. However, successful ignition became increasingly unlikely as longer inter-pulse dwells or fewer pulses provided less opportunity for flame front enhancement by successive low-impedance discharges. For PRF below 5 kHz, successful ignition at was no longer possible at this lean condition.

5. Conclusion

Three discharge modes of TPI for combustion in one atmosphere quiescent CH_4-air mixtures were identified using a pin-to-pin electrode configuration and they are high-impedance streamer, transient spark, and low-impedance spark. Schlieren images of the ignition events initiated by streamer or spark discharges were correlated with the pressure traces and showed that the transient spark or spark modes were necessary to achieve successful ignition for combustion. For single-pulse ignition, the transient spark discharge employs less than a third of the energy and Coulomb transfer compared to low-impedance spark and is hence the mode when the MIE is obtained. When the ignition energy provided by the transient plasma is close to the MIE, the ignition kernel may expand asymmetrically, which does not show significant difference in the overall combustion performance in terms of the P_{peak} and delay time from the symmetric development of the kernel. The equivalence ratio of the gas mixture impacts the combustion performance greatly; the P_{peak} decreases, and the delay time increases with ϕ decreasing from 1.0 to 0.6. The application of a 10-pulse sequence at 10 kHz extends the lean limit of $\phi = 0.6$ for single-pulse ignition to $\phi = 0.5$, allowing leaner combustion. A simplified energy deposition model demonstrated that early kernel growth was augmented by gas expansion from post-ignition discharges that ultimately led to a more robust flame kernel at the leanest equivalence ratios. More systematic studies are needed to understand the memory effect induced by high frequency repetitive pulses in sustaining the ignition kernel in streamer and spark modes to optimize pulsed power strategies for combustion ignition.

Data availability statement

All data that support the findings of this study are included within the article (and any supplementary files).

Acknowledgments

This material is based upon work supported by the Air Force Office of Scientific Research of the United States of America (AFOSR) under Award Number FA9550-22-1-0428 and in part by the U.S. Department of Energy, Office of Science, Office of Fusion Energy Sciences, under Award Number DE-SC0024623. Sandia National Laboratories is a multi-mission laboratory managed and operated by National Technology and Engineering Solutions of Sandia, LLC, a wholly owned subsidiary of Honeywell International Inc., for the U.S. Department of Energy's National Nuclear Security Administration under Contract DE-NA0003525.

ORCID iDs

Chunqi Jiang https://orcid.org/0000-0001-8895-2580
Akash C Dhotre https://orcid.org/0009-0001-3201-2669
Meimei Lai https://orcid.org/0000-0002-3325-9890
James R MacDonald https://orcid.org/0009-0007-6746-5135

References

[1] European Commission 2023 *CO_2 Emission Performance Standards For Cars and Vans* (European Commission) (available at: https://Climate.Ec.Europa.Eu/Eu-Action/Transport/Road-Transport-Reducing-Co2-Emissions-Vehicles/Co2-Emission-Performance-Standards-Cars-And-Vans_En)
[2] EPA 2021 *Revised 2023 And Later Model Year Light-Duty Vehicle Greenhouse Gas Emissions Standards* ed E.P. Agency (Federal Register)
[3] Leach F, Kalghatgi G, Stone R and Miles P 2020 The scope for improving the efficiency and environmental impact of internal combustion engines *The Scope For Improving The Efficiency And Environmental Impact Of Internal Combustion Engine* 1 100005
[4] Reitz R D 2019 IJER editorial: the future of the internal combustion engine *Int. J. Engine Res.* **21** 3–10
[5] Macdonald J R, White L, Ekoto I, Pickett L, Oh H and Han D 2023 Characterization of high-tumble flow effects on early injection for a lean-burn gasoline engine *SAE Technical Paper* 2023–01-0238 p 16
[6] Laichter J and Kaiser S A 2023 Optical investigation of the influence of in-cylinder flow and mixture inhomogeneity on cyclic variability in a direct-injection spark ignition engine *Flow Turbul. Combust.* **110** 171–83
[7] Choi Y H and Hwang J 2023 Review on plasma-assisted ignition systems for internal combustion engine application *Energies* **16** 1604
[8] Yu S and Zheng M 2021 Future gasoline engine ignition: a review on advanced concepts *Int. J. Engine Res.* **22** 1743–75
[9] Maly R and Vogel M 1979 Initiation and propagation of flame fronts in lean Ch4-air mixtures by the three modes of the ignition spark *Symp. Combust.* **17** 821–31

[10] Ziegler G F W, Wagner E P and Maly R R 1985 Ignition of lean methane-air mixtures by high pressure glow and Arc discharges *Symp. Combust.* **20** 1817–24
[11] Wang F, Jiang C, Kuthi A and Gundersen M A 2004 Transient plasma ignition of hydrocarbon-air mixtures in pulse detonation engeines *42nd AIAA Aerospace Sciences Meeting and Exhibit* (*Reno, Nevada*)
[12] Wang F, Liu J B, Sinibaldi J, Brophy C, Kuthi A, Jiang C, Ronney P and Gundersen M A 2005 Transient plasma ignition of quiescent and flowing air/fuel mixtures *IEEE Trans. Plasma Sci.* **33** 844–9
[13] Singleton D, Pendleton S J and Gundersen M A 2011 The role of non-thermal transient plasma for enhanced flame ignition in C2h4-air *J. Phys. D: Appl. Phys.* **44** 022001
[14] Shiraishi T, Urushihara T and Gundersen M 2009 A trial of ignition innovation of gasoline engine by nanosecond pulsed low temperature plasma ignition *J. Phys. D: Appl. Phys.* **42** 135208
[15] Dunn I, Ahmed K A, Leiweke R J and Ombrello T M 2021 Optimization of flame kernel ignition and evolution induced by modulated nanosecond-pulsed high-frequency discharge *Proc. Combust. Inst.* **38** 6541–50
[16] Sjöberg M, Zeng W, Singleton D, Sanders J M and Gundersen M A 2014 Combined effects of multi-pulse transient plasma ignition and intake heating on lean limits of well-mixed E85 disi engine operation *SAE Int. J. Engines* **7** 1781–801
[17] Umstattd R and Jiang C 2023 Repetitive multi-pulses enabling lean Ch4-air combustion using surface discharges *SAE Int. J. Engines* **16** 1081–91
[18] Pai D Z, Lacoste D A and Laux C O 2010 Nanosecond repetitively pulsed discharges in air at atmospheric pressure—the spark regime *Plasma Sources Sci. Technol.* **19** 065015
[19] Alderman D, Tremble C, Singleton D, Sanders J and Jiang C 2021 Effects of pulse rise time and repetition frequency on nanosecond pulsed plasma ignition for combustion *Plasma Res. Express* **3** 014001
[20] Lefkowitz J K, Hammack S D, Carter C D and Ombrello T M 2021 Elevated oh production from Nphfd and its effect on ignition *Proc. Combust. Inst.* **38** 6671–8
[21] Kim J, Gururajan V, Scarcelli R, Biswas S and Ekoto I 2022 Modeling nanosecond-pulsed spark discharge and flame Kernel evolution *J. Energy Resour. Technol. Trans. ASME* **144** 022305
[22] Sanders J, Jiang C, Kuthi A and Gundersen M A 2008 Broadband power measurement of high-voltage, nanosecond electric pulses for biomedical applications *2008 IEEE Int. Power Modulators And High-Voltage Conf.* (*Las Vegas, NV, USA*) pp 350–3
[23] Rahman M Z, Oshin E A and Jiang C 2022 Initial investigation of the streamer to spark transition in a hollow-needle-to-plate configuration *IEEE Trans. Plasma Sci.* **50** 1942–7
[24] Starikovskaia S M 2014 Plasma-assisted ignition and combustion: nanosecond discharges and development of kinetic mechanisms *J. Phys. D: Appl. Phys.* **47** 353001
[25] Akram M 1996 Two-dimensional model for spark discharge simulation in air *AIAA J.* **34** 1835–42
[26] Jiang C and Carter C 2014 Absolute atomic oxygen density measurements for nanosecond-pulsed atmospheric-pressure plasma jets using two-photon absorption laser-induced fluorescence spectroscopy *Plasma Sources Sci. Technol.* **23** 065006

DETERMININING THE ELECTRIC FIELD IN A 10-NS PULSED PLASMA IN A METHANE-AIR MIXTURE USING E-FISH

Md Ziaur Rahman[1,2], Christopher J. Kliewer[3], and Chunqi Jiang[1,2]

[1]*Department of Electrical and Computer Engineering*
[2]*Frank Reidy Research Center for Bioelectrics, Old Dominion University Norfolk, VA 23529, USA*
[3]*Sandia National Laboratoires, Livermore, CA 94550, USA*

The development of efficient and reliable ignition systems for lean fuel-air mixtures is crucial for transportation, electricity production, and other heavy industries relying on combustion. Transient plasma ignition (TPI) utilizing highly non-equilibrium plasmas, produced by nanosecond high-voltage pulses, was shown to improve lean-fuel combustion performance and reduce emission [1-2]. The transient plasma produces reactive chemical species that can significantly impact kinetics of chain reactions, reducing ignition delay time and enabling lean burn combustion (e.g., equivalence ratio, $\phi < 0.7$) [3]. The local reduced electric field controls this kinetic enhancement and measuring its distribution and dynamics will serve to inform microkinetic models and benchmark simulations. In this study, we determine the temporally resolved electric field distribution in a transient plasma driven by a 10-ns FWHM voltage pulse using a pin-to-pin electrode configuration in a quiescent atmospheric pressure CH_4/air mixture. E-field induced second harmonic generation (E-FISH) is used for the spatial and temporally resolved quantification of the E-field in different modes of the discharge for different equivalent ratios. Calibration of E-FISH to determine the absolute electric field strength is also discussed.

[1] R. J. Umstattd and C. Jiang, "Repetitive Multi-pulses Enabling Lean CH_4-Air Combustion Using Surface Discharges", *SAE International Journal of Engines,* 16.03-16-08-0061 (2023)
[2] D. Alderman *et al.* "Effects of pulse rise time and repetition frequency on nanosecond pulsed plasma ignition for combustion", *Plasma Research Express* 3.1 (2021)
[3] D. Singleton *et al.* "The role of non-thermal transient plasma for enhanced flame ignition in C2H4–air", *Journal of Physics D: Applied Physics,* 44.2 (2010)

* This material is based upon work supported by the Air Force Office of Scientific Research of the United States of America (AFOSR) under award number FA9550-22-1-0428 and by the U.S. Department of Energy, Office of Science, Office of Fusion Energy Sciences, under award number DE-SC0024623 and DE-NA0003525. This research used resources of the Low Temperat ure Plasma Research Facility at Sandia National Laboratories, which is a collaborative research facility supported by the U.S. Department of Energy, Office of Science, Office of Fusion Energy Sciences.

Impact of the dielectric surface on the electric field in a 10-ns transient plasma in a CH_4-air mixture

Md Ziaur Rahman[1,2], Christopher J. Kliewer[3], and Chunqi Jiang[1,2]

[1]*Department of Electrical and Computer Engineering*
[2]*Frank Reidy Research Center for Bioelectrics, Old Dominion University Norfolk, VA 23529, USA*
[3]*Sandia National Laboratoires, Livermore, CA 94550, USA*

Transient plasma ignition (TPI) initiated by nanosecond high-voltage pulses was shown to improve combustion efficiency and reduce the NO_x production due to its lean burn capability and the volumetric ignition effect [1]. Having a sufficiently large ignition kernel is important to reliably achieve successful combustion in extremely lean-fuel mixtures. A recent study showed that a repetitive nanosecond pulsed surface discharge could initiate sufficiently large ignition kernel without requiring an impractically high peak voltage and hence bear good economy in the ignition technology for internal combustion engines [1]. This study examines the transient electric field prior to the discharge breakdown or development of ignition kernel, and during the streamer mode of the discharge. We compare the field strength and distribution with and without the presence of a dielectric surface using a pin-to-pin electrode configuration in a CH_4/air mixture at the atmospheric pressure, obtained with the spatiotemporally-resolved, electric field-induced second harmonic generation (EFISH) method. Effects of the discharge modes and the time interval between pulses on the electric field in the surface discharge are also discussed.

[1] Ryan J. Umstattd and Chunqi Jiang, "Repetitive Multi-pulses Enabling Lean CH_4-Air Combustion Using Surface Discharges", *SAE International Journal of Engines,* 16.03-16-08-0061 (2023)

---

* This material is based upon work supported by the Air Force Office of Scientific Research of the United States of America (AFOSR) under award number FA9550-22-1-0428 and by the U.S. Department of Energy, Office of Science, Office of Fusion Energy Sciences, under award number DE-SC0024623 and DE-NA0003525. This research used resources of the Low Temperat ure Plasma Research Facility at Sandia National Laboratories, which is a collaborative research facility supported by the U.S. Department of Energy, Office of Science, Office of Fusion Energy Sciences.

Determining the electric field in a 10-ns pulsed discharge in a CH_4-air mixture using EFISH.

Md Ziaur Rahman[1,2], Christopher J. Kliewer[3], and Chunqi Jiang[1,2]

[1]*Department of Electrical and Computer Engineering*
[2]*Frank Reidy Research Center for Bioelectrics, Old Dominion University Norfolk, VA 23529, USA*
[3]*Sandia National Laboratoires, Livermore, CA 94550, USA*

Transient plasma ignition (TPI) uses repetitive nanosecond high voltage pulses for combustion ignition, enables extreme lean combustion, and reduces emission [1]. A recent study on the modes of the discharge during TPI determined that a transient spark mode of the discharge was essential to achieve combustion with a minimal ignition energy [2]. To understand the mode of the discharge, determining the electric field prior to the mode transition is hence critical. In this study, we determine the spatiotemporally resolved electric field in a 10-ns pulsed plasma using a pin-to-pin electrode configuration in the CH_4/air mixture with various equivalence ratios (ϕ) at atmospheric pressure. The electric field-induced second harmonic generation (EFISH) method was used for the study. After a series of calibrations for both the field strength and the impact of gas composition, the absolute electric field strength ranging from 10 kV/cm to 80 kV/cm was measured for the transient plasma in a lean fuel mixture. The maximum electric field was observed during the rising phase of the voltage pulse and corresponded to the time with $\sim$90% of the maximum voltage. During the discharge mode transition, the maximum electric field was found to be occurred slightly earlier for richer mixture (e.g., ϕ=0.8) compared to the leaner one ($\phi = 0.4$). Effects of the discharge mode and the time interval between pulses on the electric field in TPI are discussed.

[1] R. J. Umstattd and C. Jiang, "Repetitive Multi-pulses Enabling Lean CH_4-Air Combustion Using Surface Discharges", *SAE International Journal of Engines,* 16.03-16-08-0061 (2023)
[2] C. Jiang *et al.,* "On the modes of nanosecond pulsed plasmas for combustion ignition of quiescent CH_4-air mixtures", Journal of Physics D: Applied Physics, 2024, In press.

---

* This material is based upon work supported by the Air Force Office of Scientific Research of the United States of America (AFOSR) under award number FA9550-22-1-0428 and by the U.S. Department of Energy, Office of Science, Office of Fusion Energy Sciences, under award number DE-SC0024623 and DE-NA0003525. This research used resources of the Low Temperat ure Plasma Research Facility at Sandia National Laboratories, which is a collaborative research facility supported by the U.S. Department of Energy, Office of Science, Office of Fusion Energy Sciences.